Corals through the light : phylogenetics, functional diversity and adaptive strategies of coral-symbiont associations over a large depth range

Rodrigues Frade, P.

Publication date
2009

Document Version
Final published version

Chapter 3

In situ photobiology of corals over large depth ranges: A multivariate analysis on the roles of environment, host, and algal symbiont

PR Frade, P Bongaerts, AJS Winkelhagen, L Tonk and RPM Bak

Published in *Limnology and Oceanography* 53: 2711-2723 (2008)

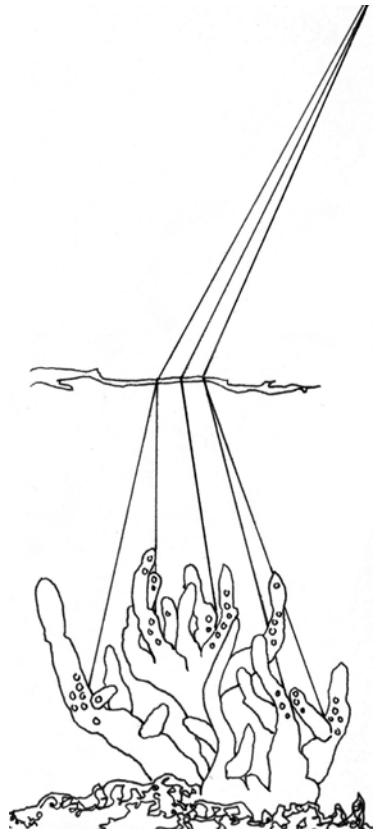

Abstract

We applied a multivariate analysis to investigate the roles of host and symbiont on the *in situ* physiological response of genus *Madracis* holobionts towards light. Across a large depth gradient (5-40 m) and for four *Madracis* species and three symbiont genotypes, we assessed several variables by measuring chlorophyll *a* fluorescence, photosynthetic pigment composition, or symbiont population descriptors. Most of the variation is explained by two major photobiological components: light-use efficiency and symbiont cell densities. Two other minor components emphasize photoprotective pathways and light-harvesting properties such as secondary pigments. Statistics highlight the role of irradiance on coral physiology and reveal mechanisms that are either genetically constrained, such as symbiont cell sizes, or environmentally dependent, such as photochemical efficiencies. Other parameters, such as cellular light-harvesting and photoprotective pigment concentrations, are regulated by host, symbiont, and environment. The interaction between host and environment stresses the role of host properties in adjusting the internal environment available for the endosymbionts. Different holobiont strategies, relating to symbiont cell density, vary in their physiological optimization of light-harvesting or photoprotective mechanisms and link to host-species distribution and dominance over the reef slope. Symbiont functional diversity appears to have a significant role but does not explain host vertical distribution patterns *per se*, highlighting the importance of species-specific morphological and physiological properties of the coral host.

Introduction

Reef-building corals thrive across large depth ranges through adaptation to a broad set of environmental gradients, the most important of which is light (Veron 2000). The success of symbiotic corals under different light regimes depends on the integrated physiological capacity of the symbiotic partners: the animal host and the phototrophic dinoflagellate endosymbiont (genus *Symbiodinium*), together: the holobiont (Trench 1993). Their adaptations to the environment ultimately relate to the resilience of coral reefs as these are affected by a rapidly changing environment (Hoegh-Guldberg *et al.* 2007).

Most scleractinian coral species have limited vertical distributions (Veron 2000) that relate to specific adaptations to available light, such as relative ratios of heterotrophic and autotrophic components (Anthony and Fabricius 2000) or different respiration rates (McCloskey and Muscatine 1984). The phototrophic component of the association is thought to play a major role in coral niche occupation. Specifically, *Symbiodinium* functional diversity has been hypothesised to regulate the vertical distribution of corals (Iglesias-Prieto and Trench 1994; Iglesias-Prieto *et al.* 2004).

The genus *Symbiodinium* is a taxonomically diverse group, as recently confirmed by several molecular markers (reviewed by Coffroth and Santos 2005). Phylogenies such as those based on nuclear ribosomal deoxyribonucleic acid (rDNA) divide the genus into several large clades (Rowan and Powers 1991a). The internal transcribed spacer regions 1 and 2 (ITS1 and ITS2) further characterize numerous subcladal genetically distinct types (LaJeunesse 2001; van Oppen *et al.* 2001a), which closely approximate physiologically and ecologically distinct populations (LaJeunesse 2002; Warner *et al.* 2006; Frade *et al.* 2008c).

Symbiodinium, as a genus, can be adapted to distinct light regimes, but also shows photoacclimation potential. This allows for the extension, within certain genetic constraints, of the limits of environmental tolerance (Iglesias-Prieto and Trench 1994). Several photoacclimation mechanisms have been reported, including cellular photosynthetic pigment quality and quantity variation (e.g. Titlyanov 1981). For instance, amounts of chlorophyll-protein complexes are known to increase as light availability decreases (Iglesias-Prieto and Trench 1997b). This increase contributes to the enhancement of light harvesting and contrasts with photoprotective mechanisms, which become active to avoid overexcitation of the photosynthetic system. Photoprotective pathways compete with photochemistry for the deactivation of chlorophyll *a* (Chl *a*) excited states leading to heat dissipation (Muller *et al.* 2001). This phenomenon, known as nonphotochemical quenching (NPQ), constitutes a mechanism against damaging effects of excess light energy and photo-oxidative stress. One of the mechanisms that trigger NPQ is the xanthophylls cycle, involving carotenoid pigments that, under high light, are rapidly converted from the harvesting form into the protective form. In dinoflagellates, these two forms correspond to diadinoxanthin and its di-epoxide congener, diatoxanthin, respectively (Brown *et al.* 1999; Warner and Berry-Lowe 2006). Photosynthetic processes such as NPQ have been commonly investigated by means of fluorescence measurements of photosystem II (PSII), which are remarkably informative regarding processes that affect both the light-harvesting antennae and electron-transfer chains (Gorbunov *et al.* 2001; Iglesias-Prieto *et al.* 2004). Besides symbiont-driven processes, there are host-related mechanisms thought to contribute to an efficient photosynthetic activity. These include mechanisms such as polyp behaviour (Levy *et al.* 2006a), changes in skeletal

morphology (Enriquez *et al.* 2005) or host pigment composition (Schlichter *et al.* 1994; Salih *et al.* 2000).

The coral genus *Madracis* Milne Edwards and Haime 1849 has a wide depth distribution, ranging from *c*. 2 to > 100 m on Caribbean reefs (Wells 1973a; Vermeij and Bak 2002), and includes species with very distinct depth-distribution patterns (Vermeij and Bak 2003). Despite the large depth range covered, all specimens sampled to date only harbour clade B *Symbiodinium* (Diekmann *et al.* 2002). Frade *et al.* (2008c) described three *Symbiodinium* ITS2 types in the *Madracis* genus. Type B7 *Symbiodinium* is a generalist, occurring in all *Madracis* species at all depths. Type B13 is restricted to the shallow-water specialist *Madracis mirabilis*. Type B15 is typical of deep reef environments. Contrasting with symbiont variation over depth, Frade *et al.* (2008c) found no variation over colony surfaces. Their study suggested depth-based ecological function and host specificity for *Symbiodinium* ITS2 types in *Madracis*. However, the mechanisms behind such diversity are unknown.

Due to the distinct vertical distribution patterns and the variety of depth-specific *Symbiodinium* types, the genus *Madracis* provides an appropriate model to study the photobiological adaptation and plasticity of coral hosts and symbionts over large depth ranges. Our objective is to understand the role of functional diversity in coral-algal symbioses, and ultimately explain coral depth distribution. The questions we pose here are: What is the physiological plasticity of *Madracis* holobionts across depths? What is the role of the coral host and symbiont types in the response of the holobiont?

Most studies on the photophysiology of coral-algal associations either look at a reduced set of variables or analyse each variable separately. The intrinsic consequence of the last type of analysis is that it overlooks common patterns between distinct variables, or it produces false positives due to multiple statistical comparisons. In this study, we extensively address coral holobiont photoacclimation and adaptation by measuring *in situ* photosynthetic activity, pigment composition, symbiont densities and cell sizes for different host species across a large depth range. We apply an innovative multivariate approach to reveal underlying processes involved in the adaptation of corals and their symbionts to the coral reef environment. We describe distinct photobiological mechanisms, either driven by the environment or genetically constrained by different holobiont associations.

Materials and methods

Study area

Fieldwork was conducted on Curaçao, southern Caribbean (*see* Figure 2.1, in Chapter 2) from July to September 2005. We surveyed *c*. 2000 m^2 of the Buoy One reef location, a previously well-studied site (e.g. Bak 1977; Vermeij *et al.* 2007b). The study site's depth-mediated light attenuation, light spectral distribution, and seawater temperature were characterised during the sampling period (Frade *et al.* 2008c).

Species

Four *Madracis* morphospecies with distinct depth distributions (Vermeij and Bak 2003), *Madracis mirabilis*, *Madracis pharensis*, *Madracis senaria* and *Madracis formosa*, were included in this study. The encrusting or submassive *M. pharensis* (Heller 1868) and *M.*

senaria (Wells 1973a) are found across all depths (5 to > 60 m); the branching species *M. mirabilis* Duchassaing and Michelotti 1861 and *M. formosa* (Wells 1973a) are restricted to, respectively, shallow- (2 to 25 m) and deep-water (> 30 m) habitats.

Sampling approach

Corals were sampled at four depths (5, 10, 25 and 40 m) and for two different surface positions: horizontal top ($\alpha = 0°$) and seaward-facing vertical side ($\alpha = 90°$), except for 40-m depth (where only top was sampled). Two hundred and thirty samples were collected from 131 coral colonies. For details on sample size for species, depths and surface position, *see* Table 3.1. Care was taken to sample only adult, healthy, fully pigmented, light-exposed colonies.

Light environment

Because we included only light-exposed colonies, we can assume depth to be a proxy for light. Nevertheless, incident irradiance was measured for about one-third of the sampled colonies (for $\alpha = 0°$ and $\alpha = 90°$) using a photosynthetic active radiation (PAR: 400-700 nm) cosine-corrected LI-192SA light sensor (Li-Cor). The measurements, taken under conditions of minor cloud cover and no wind, were standardised to the irradiance value measured in the open water column at the same occasion and homologous depth to correct for meteorological bias (Vermeij and Bak 2002).

Fluorescence measurements

All fluorescence measurements were taken *in situ* using an underwater pulse amplitude-modulated fluorometer (Diving-PAM, Walz) on days with low cloud cover. By using an opaque plastic fibre-optics holder, we were able to standardize the distance between the fibre-optics tip and the coral surface (10 mm) and avoid environmental light exciting the sampled area. All midday measurements were preceded by 1 min of dark acclimation to completely relax photochemical quenching (Iglesias-Prieto *et al.* 2004).

Maximum excitation pressure over PSII - For each coral colony, the effective quantum yield of PSII ($\Delta F : Fm'$) was recorded at solar noon (± 30 min), and the maximum PSII quantum yield ($Fv : Fm$) was measured at the preceding dusk (*Ynoon* and *Ydusk*, respectively). The maximum light excitation pressure over PSII (Q_m) was calculated as in Iglesias-Prieto *et al.* (2004): $Q_m = 1 - [(\Delta F : Fm')/(Fv : Fm)]$. As Q_m approaches 1.0, higher percentages of PSII reaction centres are closed.

Photosynthesis vs. irradiance (PE) curve parameters - Effective quantum yield (Y) was measured at solar noon (± 30 min) during "rapid light curves", consisting of eight successive PAR irradiance levels (each 30 s in duration). PE curves were built using relative *ETR* (electron transfer rate) as photosynthetic rate estimator: $ETR = Y$ x PAR x 0.5. The respective PAR levels used for calculations were calibrated daily and include a correction for the fluorometer battery-power reduction. The following parameters were derived from the PE curves (Iglesias-Prieto and Trench 1994): *alpha*, or the photosynthetic efficiency at subsaturating irradiances, calculated as the linear regression of the light-limited photosynthetic rates (including the lowest three PAR levels); *ETRmax*, or the maximum photosynthetic rate, calculated as the average of the two highest *ETR* points; and E_k, or the light saturation parameter, calculated as

ETRmax : *alpha*.

Coral collection and processing

Corals were collected immediately after midday fluorescence measurements or, rarely, 24 h later. Each colony was sampled contiguously to the area used for fluorescence recordings, or in the closest branch (in *M. mirabilis* and *M. formosa*). Coral fragments were collected with hammer and chisel and placed in seawater-filled plastic bags that were kept in dark and transported at environmental temperature to the laboratory. Coral tissue was completely removed from a *c*. 1-4-cm^2 subsample using a WaterPik® jet of 0.2-μm-filtered seawater. The slurry was passed through a 20-μm nylon filter to remove skeletal debris and small epifauna, and its total volume was determined (usually *c*. 200 mL). For pigment analyses, a subsample of homogenised blastate was loaded on 0.45-μm cellulose acetate membrane filters (Schleicher and Schuell) that were immediately frozen and kept in liquid nitrogen. Filters were later freeze-dried and stored at -80ºC for subsequent analyses.

For symbiont population descriptors, the remainder homogenised blastate was vortexed for 5 min to loosen algal cells. Replicate subsamples were concentrated and fixed in glutaraldehyde (0.5% final concentration), kept 10 min in the dark, and were then frozen in liquid nitrogen to be later stored at -80ºC for cell-density determination. For cell-size measurements, another subsample was photographed for a minimum of 100 symbiont cells under a Zeiss microscope (against a size grid).

For standardizations, the polypary surface area of the fragments was estimated (with less than 4% error) using the aluminium-foil method (Marsh 1970). Polyp density was determined for the same skeletal area.

Symbiont population descriptors

Cell sizes - The maximum cell diameter was digitally determined for a minimum of 100 single symbiont cells per sample using the software IMAGE J. Only samples originated from the horizontal top ($\alpha = 0°$) colony position were analysed.

Cell densities - Symbiont cell densities were determined in an Epics XL-MCL Beckman Coulter flow cytometer. After thawing and rehomogenization, 122.2 μL of a glutaraldehyde-fixed replicate per sample were incorporated in the flow cytometer, and algal cells counted, from which densities were calculated. These were shown by a pilot test to be on average 3.6% lower than densities determined by microscopy on the same samples.

Pigment analyses

Photosynthetic pigment composition was analysed in a Millipore-Waters high-performance liquid chromatography (HPLC) system. Pigments were first extracted by ultra-sonification in 2 mL of solvent (95% methanol, 2% ammonium acetate), and 100 μL of the filtered mobile phase was injected in the HPLC pumping device. All steps were performed for only one sample each time and at ice-cold conditions. Pigment concentrations were calculated after integration of the 436-nm absorbance peak areas (WATERS EMPOWER 2 software) by linear extrapolation using conversion factors determined by running Sigma pigment standards in the same HPLC system (except for dinoxanthin, for which the conversion factor was estimated by assuming

a similar molar extinction coefficient as diadinoxanthin and correcting it with respect to the difference in molecular weight). Results were corrected for changes in the chromatography partitioning conditions as monitored by regularly injecting standards.

The following photosynthetic pigments were present in all samples: chlorophyll *a* (Chl *a*), chlorophyll c_2 (Chl c_2) and the carotenoids peridinin, dinoxanthin, diadinoxanthin, diatoxanthin, and *β*,*β*-carotene. Residual amounts (< 1% Chl *a*) of chlorophyll c_1, pheophytin, pheophorbide, zeaxanthin, and chlorophyll *b* were detected in some of the samples. Because samples were kept in the dark for 1-2 h before fixation, individual xanthophyll levels are not reliable (diatoxanthin converted to diadinoxanthin by epoxidation; Muller *et al.* 2001). Therefore, only the value for the total xanthophyll-cycle pool (sum of diadinoxanthin and diatoxanthin), was included in the analyses. All photosynthetic pigments were highly correlated to Chl *a* amounts, and therefore they were normalised to Chl *a* prior to analyses. Other Chl *a*-based normalizations were applied, such as for photosynthetic rates. Other normalizing divisors used were coral surface area (Chl *a* area^{-1}), symbiont cell density (Chl *a* cell^{-1}, *ETRmax* cell^{-1}, and *alpha* cell^{-1}), and symbiont cell volume (Chl *a* cellvol^{-1}), which we calculated using the measured cell diameter and assuming sphere-shaped cells.

Genetic analyses

An *c.* 4-cm^2 subsample of each collected coral fragment was used for the genetic characterization of the *Symbiodinium* rDNA ITS2 type(s) present. For methods and results, *see* Frade *et al.* (2008c).

Statistics

Multiple linear regressions were used to analyse (log-transformed) colony surface incident irradiance data.

All photobiological data were incorporated in a principal component analysis (PCA) in order to adequately reduce the dimensionality of the data set and identify processes that differ in their regulation. log-transformations were applied when necessary to improve linearity and reduce outlier effect. Percentage data (pigment ratios) were instead arcsin transformed. Variables were normalised before analyses, and samples containing missing data were excluded. The principal components (PCs) to be retained were those showing variances exceed 1 (the average variance of PCs for a correlation-based analysis) (Zuur *et al.* 2007).

To improve interpretability, we applied a simplified component technique based on the least absolute shrinkage and selection operator (SCoTLASS, Jolliffe *et al.* 2003), which aims to produce uncorrelated modified components with unambiguously strong (positive or negative loadings) or weak correlation (zero loadings) to the original variables. SCoTLASS components (SCs) were computed for several tuning parameter (*t*) values, representing different levels of simplification. As simplicity increases (lower *t*), the variation accounted for by the first components decreases. This process runs till a suitable trade-off between interpretability and variation explained was achieved. The resulting SCoTLASS loadings were used to manually compute new scores for every sample, for each respective retained component. The SCs were then used as response variables in separate multiple linear regression models to assess the significance of explanatory variables: host species, depth, colony surface position, and symbiont ITS2 type. All statistical tests were performed at a significance level of 0.05, and

P-values were adjusted according to Bonferroni correction. Modelling was carried out with the software BRODGAR linked to the statistics package R.

RESULTS

Light environment

The standardised irradiance data measured over 35 colonies (for α = 0° and α = 90°, different species and depths) show no difference in exposure of colonies to light between coral species ($F_{3,64} = 1.2624$, $P = 0.295$). We therefore exclude any influence of the external light environment on the species differences found. There is a significant interaction between depth and surface position on the amount of light reaching the colonies ($F_{1,66} = 32.248$, $P < 0.001$). Figure 3.1 shows that this pattern closely resembles the depth-based light attenuation as measured in the water column (Frade *et al.* 2008c). On average, the colony incident PAR irradiance is 94.4% of the value measured in the water column, but there is no statistical difference between these two data sets ($F_{1,147} = 2.7795$, $P = 0.098$). This shows that depth is a good proxy for light and that there is no relevant influence of reef topography within each sampling depth in our data set (but *see* Vermeij and Bak 2002).

Photobiology

Table 3.1 shows symbiont population descriptors, photosynthetic pigment composition, coral polyp densities, and all fluorescence-based data for a total of 230 samples grouped by colony surface position, host species and depth. The data was summarised in 21 different variables representing distinct photobiological processes, some of which are alternative expressions of the same data (*see* Table 3.1 for abbreviations). Symbiont ITS2 types identified for the same samples (Frade *et al.* 2008c) are also shown. Pigment data resemble previously reported values (Apprill *et al.* 2007), except for the relatively higher ratios to Chl *a* that we measured

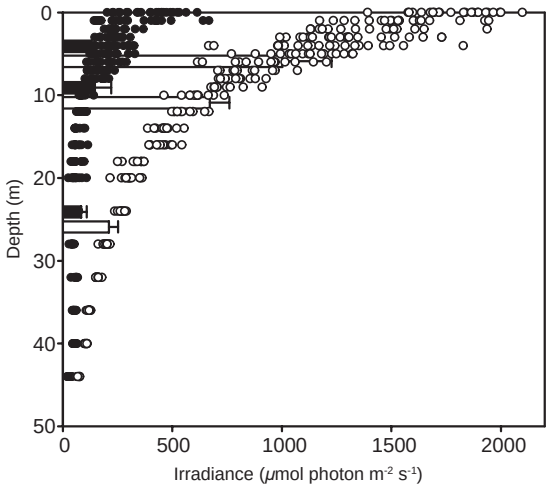

Figure 3.1 Colony incident PAR irradiance (bars) and water-column PAR irradiance (circles) for two directions: straight from above (α = 0°, open) and from aside into the reef (α = 90°, closed). Water-column irradiance is modified after Frade *et al.* (2008c).

Table 3.1 *Madracis* spp. photobiological data (average ± SD, sample size indicated in parentheses) for two different colony surface positions (top and side) and across depth (5, 10, 25 and 40 m). Symbiont type, taken from Frade *et al*. (2008c), represents percentage of colonies harbouring a certain *Symbiodinium* rDNA ITS2-type (total percentage exceeds 100% if two types co-occurred). Abbreviations stand for: Chl *a* area^{-1} – chlorophyll *a* contents per surface area, Chl *a* cell^{-1} – chlorophyll *a* contents per symbiont cell, Chl *a* cellvol^{-1} – chlorophyll *a* contents per cell volume, Chl c_2 – chlorophyll c_2, xanthophylls – xanthophyll-cycle pool size, *Ydusk* – maximum quantum yield of PSII (or *Fv* : *Fm*), *Ynoon* – effective quantum yield of PSII (or ΔF : *Fm'*), Q_m – maximum light excitation pressure over PSII, *ETRmax* - maximum photosynthetic rate (based on relative *ETR*), *alpha* - photosynthetic efficiency at subsaturating irradiances, E_k - light saturation parameter (or *ETRmax alpha*$^{-1}$).

Position	Species	Depth (m)	Symbiont type Frade *et al.* (2008)	Cell density (x10^{6}cells cm^{-2})	Cell size (μm)	Chl *a* area^{-1} (μg cm^{-2})	Chl *a* cell^{-1} (pg cell^{-1})
Top	*M. mirabilis*	5	B7 (36%), B13 (73%) (11)	1.8±0.3 (11)	8.8±1.5 (6)	3.7±1.1 (11)	2.1±0.6 (11)
		10	B7 (33%), B13 (92%) (12)	1.7±0.4 (12)	8.3±0.2 (6)	5.2±1.4 (12)	3.2±0.8 (12)
		25	B7 (40%), B13 (90%) (10)	1.6±0.3 (10)	8.2±0.3 (6)	5.6±1.3 (10)	3.7±0.9 (10)
	M. pharensis	5	B7 (100%) (11)	3.0±1.0 (11)	8.6±0.2 (6)	9.9±5.6 (11)	3.2±1.2 (11)
		10	B7 (100%) (15)	2.3±0.9 (12)	8.5±0.4 (9)	6.6±2.2 (12)	3.0±0.8 (12)
		25	B7 (54%), B15 (46%) (13)	2.0±0.9 (11)	9.3±1.1 (6)	10.3±3.9 (10)	5.6±2.2 (10)
		40	B7 (36%), B15 (64%) (11)	1.8±0.8 (11)	9.9±1.1 (9)	14.0±4.2 (11)	8.5±3.2 (11)
	M. senaria	5	B7 (90%), B13 (10%) (10)	2.8±0.8 (10)	9.1±0.4 (8)	8.5±2.6 (10)	3.1±0.6 (10)
		10	B7 (100%) (11)	2.5±1.0 (10)	9.5±1.5 (6)	8.4±3.4 (10)	3.7±1.3 (10)
		25	B7 (100%) (10)	2.9±0.6 (10)	8.8±0.3 (6)	13.5±2.0 (10)	4.8±1.1 (10)
		40	B7 (100%) (9)	2.5±0.6 (10)	9.3±0.3 (7)	13.1±3.7 (10)	5.2±0.9 (10)
	M. formosa	40	B7 (92%), B15 (23%) (13)	1.4±0.6 (11)	9.6±0.5 (8)	9.3±3.1 (11)	7.0±2.0 (11)
Side	*M. mirabilis*	5	B7 (50%), B13 (70%) (10)	1.3±0.4 (11)		5.3±1.3 (11)	4.0±0.8 (11)
		10	B13 (100%) (12)	1.5±0.3 (12)		6.5±2.0 (12)	4.4±0.9 (12)
		25	B7 (50%), B13 (80%) (10)	1.3±0.4 (10)		6.2±1.5 (10)	4.9±0.8 (10)
	M. pharensis	5	B7 (100%) (11)	3.4±1.1 (11)		16.4±6.3 (11)	5.0±1.3 (11)
		10	B7 (93%), B15 (7%) (14)	2.6±0.8 (12)		15.1±3.6 (12)	6.3±2.2 (12)
		25	B7 (54%), B15 (46%) (13)	1.7±0.7 (11)		15.4±4.3 (10)	9.8±3.8 (10)
	M. senaria	5	B7 (100%) (10)	3.6±1.3 (10)		17.2±5.8 (10)	5.1±1.8 (10)
		10	B7 (100%) (11)	3.3±1.1 (10)		16.1±4.1 (10)	5.3±2.2 (10)
		25	B7 (100%) (11)	2.6±0.8 (10)		16.3±3.6 (10)	6.5±1.2 (10)

for the accessory pigments peridinin, Chl c_2 and dinoxanthin.

We preselected 179 samples (representing 100 colonies) containing no missing data for the PCA. Cell sizes were only determined for colony top surface position and were therefore excluded from the PCA dataset (as well as Chl *a* cellvol^{-1}). Six outliers were further removed based on single variable exploration tools. The first four PCs had variances higher than 1 and accounted for 79.9% of the variation (40.5, 22.3, 9.8 and 7.3%, respectively). Therefore, these were retained for further analyses. Figure 3.2 shows the PCA correlation biplot (n = 173) for the two first PCs (62.8% of the variation). The apparently even graphical disposition of the 19 variable axes over the first two PCs and the relatively low correlation between them do not facilitate a definite interpretation. This is unequivocally indicated by the high amount of intermediate loadings in the PCA and the low number of variables with zero loadings (Table 3.2, columns for PCs). A tentative interpretation of these loadings would be that the main source of variation in the data (represented by PC1) is between those samples that have greater than average values for variables Chl *a* area^{-1}, Chl *a* cell^{-1}, peridinin Chl *a*$^{-1}$, *Ydusk*, *Ynoon*, and *alpha*, coupled with smaller than average values for variables dinoxanthin Chl *a*$^{-1}$, xanthophylls Chl *a*$^{-1}$, Q_m, E_k, and *ETRmax* Chl *a*$^{-1}$, and those other samples showing the

Table 3.1 (*continued*)

Position	Species	Depth (m)	Chl *a* cellvol^{-1} (x10^{-3}pg μm^{-3})	Chl c_2 Chl a^{-1}	Peridinin Chl a^{-1}	β,β-carotene Chl a^{-1} (x10)	Dinoxanthin Chl a^{-1} (x10)	Xanthophylls Chl a^{-1}
Top	*M. mirabilis*	5	6.2±2.9 (6)	0.25±0.01 (11)	0.67±0.04 (11)	0.11±0.04 (11)	0.88±0.12 (11)	0.22±0.02 (11)
		10	11.5±2.8 (6)	0.25±0.01 (12)	0.70±0.03 (12)	0.13±0.03 (12)	0.78±0.08 (12)	0.21±0.02 (12)
		25	14.0±2.4 (6)	0.25±0.01 (10)	0.72±0.02 (10)	0.14±0.03 (10)	0.68±0.06 (10)	0.19±0.02 (10)
	M. pharensis	5	9.7±2.0 (6)	0.25±0.01 (11)	0.68±0.05 (11)	0.17±0.04 (11)	0.72±0.09 (11)	0.21±0.03 (11)
		10	10.2±3.5 (9)	0.25±0.01 (12)	0.69±0.05 (12)	0.15±0.04 (12)	0.69±0.09 (12)	0.20±0.02 (12)
		25	13.2±3.8 (6)	0.25±0.01 (10)	0.75±0.08 (10)	0.16±0.03 (10)	0.60±0.06 (10)	0.17±0.01 (10)
		40	17.7±8.3 (9)	0.24±0.02 (11)	0.80±0.03 (11)	0.18±0.04 (11)	0.54±0.07 (11)	0.17±0.02 (11)
	M. senaria	5	7.9±2.0 (8)	0.26±0.01 (10)	0.75±0.06 (10)	0.14±0.06 (10)	0.63±0.10 (10)	0.19±0.01 (10)
		10	8.7±3.0 (6)	0.26±0.01 (10)	0.73±0.03 (10)	0.15±0.05 (10)	0.62±0.08 (10)	0.20±0.02 (10)
		25	12.3±1.7 (6)	0.26±0.01 (10)	0.76±0.02 (10)	0.14±0.04 (10)	0.49±0.05 (10)	0.18±0.01 (10)
		40	11.3±1.3 (7)	0.26±0.02 (10)	0.78±0.04 (10)	0.12±0.03 (10)	0.44±0.04 (10)	0.17±0.01 (10)
	M. formosa	40	15.9±4.7 (8)	0.24±0.02 (11)	0.75±0.03 (11)	0.19±0.04 (11)	0.51±0.04 (11)	0.16±0.01 (11)
Side	*M. mirabilis*	5		0.26±0.01 (11)	0.75±0.02 (11)	0.11±0.05 (11)	0.60±0.12 (11)	0.18±0.02 (11)
		10		0.25±0.01 (12)	0.75±0.04 (12)	0.12±0.03 (12)	0.60±0.05 (12)	0.17±0.01 (12)
		25		0.25±0.01 (10)	0.76±0.03 (10)	0.14±0.04 (10)	0.58±0.05 (10)	0.18±0.01 (10)
	M. pharensis	5		0.26±0.01 (11)	0.71±0.04 (11)	0.14±0.04 (11)	0.59±0.08 (11)	0.18±0.02 (11)
		10		0.26±0.01 (12)	0.77±0.05 (12)	0.16±0.03 (12)	0.52±0.07 (12)	0.17±0.01 (12)
		25		0.24±0.02 (10)	0.81±0.05 (10)	0.20±0.04 (10)	0.46±0.05 (10)	0.16±0.02 (10)
	M. senaria	5		0.26±0.01 (10)	0.78±0.05 (10)	0.14±0.03 (10)	0.46±0.08 (10)	0.17±0.01 (10)
		10		0.26±0.01 (10)	0.78±0.04 (10)	0.13±0.05 (10)	0.49±0.07 (10)	0.17±0.02 (10)
		25		0.25±0.01 (10)	0.78±0.02 (10)	0.17±0.02 (10)	0.39±0.04 (10)	0.16±0.01 (10)

opposite response. Likewise, these two groups of variables are likely to be highly (negatively) correlated to each other and uncorrelated to variables such as Chl c_2 Chl a^{-1}, β,β-carotene Chl a^{-1}, polyp density, and *alpha* cell^{-1}.

The use of SCoTLASS contributed to a major increase in interpretability, as shown by the increase in the number of variables with zero loadings (Figure 3.3). A t of 2.322 was chosen for further analyses because at this high degree of simplification, the variation explained by the four first SCs was still high (70.1%). Table 3.2 (columns for SCs) shows the loadings obtained by SCoTLASS for $t = 2.322$. Now, most of the original variables load strongly in only one of the SCs, and these differ from each other in terms of the variables they represent. The number of variables with zero loadings is now 11, 13, 10 and 7, for SC1, SC2, SC3 and SC4, respectively. SC1 (representing 22.8% of the variation) is mainly correlated to variables directly linked to photochemical or photosynthetic efficiencies, such as Q_m, *alpha* or E_k. SC2 (22.6%) is strongly (negatively) correlated to symbiont cell density. The (positive) correlation to normalised *ETRmax* and *alpha* appears to be a consequence of variation in cell density because it is not accompanied by changes in the respective raw parameters (loadings of 0.00 for *ETRmax* and *alpha*). The same holds for the strong correlation of Chl *a* area^{-1}, since Chl *a* cell^{-1} is not relevant to this component (loading of 0.00). SC3 (15.8%) represents an apparently mixed assemblage including Chl *a* cell^{-1}, ratios of accessory photopigments such as peridinin Chl a^{-1}, dinoxanthin Chl a^{-1}, or xanthophylls Chl a^{-1}, and *ETRmax*. SC4 (9.0%) mainly correlates (positively) to polyp density and to other accessory pigments such as β,β-carotene Chl a^{-1} (positively) and Chl c_2 Chl a^{-1} (negatively). The correlations to the different original variables were rarely equivocal.

Table 3.1 (*continued*)

Position	Species	Depth (m)	Polyp density (no. cm^{-2})	*Ydusk*	*Ynoon*	Q_m	*ETRmax* (*µ*mol electrons m^{-2} s^{-1})
Top	*M. mirabilis*	5	24.6±4.0 (11)	0.55±0.03 (11)	0.37±0.03 (11)	0.33±0.05 (11)	64.3±12.3 (11)
		10	24.3±4.9 (12)	0.57±0.03 (12)	0.44±0.04 (12)	0.23±0.06 (12)	78.7±17.9 (11)
		25	25.0±2.5 (10)	0.61±0.02 (10)	0.49±0.06 (10)	0.20±0.08 (10)	73.3±5.5 (8)
	M. pharensis	5	29.5±5.6 (11)	0.55±0.05 (9)	0.37±0.11 (9)	0.34±0.15 (9)	65.2±7.8 (9)
		10	26.0±7.5 (12)	0.57±0.03 (11)	0.41±0.08 (11)	0.28±0.12 (11)	73.8±12.8 (10)
		25	25.0±6.9 (11)	0.62±0.03 (8)	0.54±0.07 (8)	0.14±0.09 (8)	67.9±16.1 (7)
		40	28.1±3.7 (11)	0.59±0.06 (7)	0.54±0.08 (7)	0.08±0.08 (7)	68.2±9.0 (7)
	M. senaria	5	23.8±5.5 (10)	0.50±0.04 (8)	0.32±0.09 (8)	0.36±0.15 (8)	51.7±11.3 (8)
		10	23.2±3.7 (10)	0.54±0.04 (10)	0.45±0.05 (10)	0.17±0.08 (10)	66.0±8.9 (9)
		25	20.9±7.6 (10)	0.61±0.01 (9)	0.53±0.08 (9)	0.13±0.12 (9)	63.3±10.6 (8)
		40	21.8±3.4 (10)	0.58±0.01 (7)	0.52±0.05 (7)	0.11±0.08 (7)	61.2±8.9 (7)
	M. formosa	40	33.8±4.0 (11)	0.61±0.03 (7)	0.51±0.07 (7)	0.16±0.08 (7)	59.1±11.3 (7)
Side	*M. mirabilis*	5	22.2±5.1 (11)	0.61±0.03 (11)	0.60±0.04 (11)	0.03±0.07 (11)	65.0±13.8 (11)
		10	21.7±4.7 (12)	0.62±0.02 (12)	0.61±0.01 (12)	0.02±0.03 (12)	57.3±11.0 (11)
		25	22.9±2.4 (10)	0.63±0.01 (10)	0.62±0.03 (10)	0.01±0.05 (10)	47.2±7.8 (8)
	M. pharensis	5	27.7±3.3 (11)	0.62±0.03 (9)	0.62±0.04 (9)	0.01±0.06 (9)	70.5±14.8 (9)
		10	28.8±3.7 (12)	0.62±0.03 (11)	0.61±0.05 (11)	0.01±0.05 (11)	58.3±7.4 (10)
		25	27.1±4.6 (11)	0.62±0.07 (8)	0.64±0.07 (8)	-0.03±0.02 (8)	43.6±10.9 (7)
	M. senaria	5	23.0±7.0 (10)	0.60±0.02 (8)	0.57±0.06 (8)	0.04±0.08 (8)	56.8±9.0 (8)
		10	20.5±2.7 (10)	0.61±0.02 (10)	0.61±0.03 (10)	0.00±0.04 (10)	47.6±9.3 (9)
		25	21.6±6.8 (10)	0.63±0.01 (9)	0.63±0.03 (9)	0.00±0.03 (9)	39.9±9.9 (8)

Significance of photobiological components

Figure 3.4 (a-p) shows the univariate multiple regression graphical outcomes for each of the factors tested on the new scores (one or two outliers were removed). SC1 scores increase significantly with depth ($F_{1,169} = 179.36$, $P < 0.001$; Figure 3.4a) and are significantly dependent on colony surface position ($F_{1,169} = 588.50$, $P < 0.001$; Figure 3.4b). Since SC1 negatively correlates with, for instance, Q_m (Table 3.2), the positive regressions show that the maximum light excitation over PSII decreases significantly with increasing depth and decreases from $\alpha = 0°$ to $\alpha = 90°$ colony surface position, while it is unaffected by host species (Figure 3.4c) or symbiont type (Figure 3.4d). SC2 is dependent on host species ($F_{3,168} = 80.630$, $P < 0.001$; Figure 3.4g) and surface position ($F_{1,168} = 21.084$, $P < 0.001$; Figure 3.4f). Hence, the SC2-linked symbiont cell density is significantly lower in *M. mirabilis* than in the other species, and it slightly increases from $\alpha = 0°$ to $\alpha = 90°$ surfaces within colonies, while the normalised photosynthetic activity changes in the opposite direction. SC3 scores are affected by all explanatory factors, decreasing with depth ($F_{1,162} = 76.781$, $P < 0.001$; Figure 3.4i) and from $\alpha = 0°$ to $\alpha = 90°$ colony surface positions ($F_{1,162} = 181.240$, $P < 0.001$; Figure 3.4j), being higher in *M. mirabilis* and *M. pharensis* than in *M. senaria* and *M. formosa* ($F_{3,162} = 19.568$, $P < 0.001$; Figure 3.4k), and differing between symbiont types ($F_{2,162} = 9.370$, $P < 0.001$; Figure 3.4l). This reflects, for example, that symbiont type B15 has higher Chl *a* cell^{-1} and peridinin Chl a^{-1} than types B7 and B13 *Symbiodinium*. Finally, SC4 is significantly related to host species ($F_{3,163} = 12.784$, $P < 0.001$; Figure 3.4o) and to symbiont type ($F_{2,163} = 10.991$, $P <$

Table 3.1 (*continued*)

Position	Species	Depth (m)	*alpha*	E_k (μmol photons m^{-2} s^{-1})	*ETRmax* cell^{-1} (x10^{-6} μmol electrons cell^{-1} h^{-1})	*ETRmax* Chl *a*$^{-1}$ (μmol electrons mg^{-1} Chl *a* s^{-1})	*alpha* cell^{-1}	*alpha* Chl *a*$^{-1}$ (x10)
Top	*M. mirabilis*	5	0.15±0.03 (11)	447±44 (11)	13.7±3.9 (11)	1.9±0.6 (11)	0.09±0.03 (11)	0.43±0.15 (11)
		10	0.170.04 (11)	474±38 (11)	17.4±5.4 (11)	1.7±0.7 (11)	0.10±0.03 (11)	0.35±0.14 (11)
		25	0.22±0.03 (8)	349±68 (8)	17.5±3.3 (8)	1.2±0.2 (8)	0.14±0.03 (8)	0.35±0.04 (8)
	M. pharensis	5	0.16±0.04 (9)	415±68 (9)	8.3±2.9 (9)	0.9±0.5 (9)	0.06±0.02 (9)	0.22±0.13 (9)
		10	0.19±0.04 (10)	400±49 (10)	10.3±3.0 (8)	1.0±0.3 (8)	0.07±0.03 (8)	0.26±0.08 (8)
		25	0.21±0.06 (7)	328±63 (7)	14.6±8.8 (7)	0.8±0.4 (7)	0.12±0.07 (7)	0.25±0.11 (7)
		40	0.24±0.04 (7)	290±38 (7)	20.1±8.5 (7)	0.6±0.2 (7)	0.19±0.09 (7)	0.21±0.06 (7)
	M. senaria	5	0.14±0.05 (8)	382±76 (8)	6.9±1.6 (8)	0.6±0.2 (8)	0.05±0.01 (8)	0.16±0.04 (8)
		10	0.18±0.03 (9)	374±48 (9)	11.0±4.2 (9)	0.8±0.2 (9)	0.08±0.04 (9)	0.22±0.05 (9)
		25	0.21±0.04 (8)	304±67 (8)	8.4±2.8 (8)	0.5±0.1 (8)	0.08±0.02 (8)	0.17±0.06 (8)
		40	0.24±0.03 (7)	256±48 (7)	9.5±3.6 (7)	0.5±0.2 (7)	0.10±0.03 (7)	0.20±0.06 (7)
	M. formosa	40	0.26±0.02 (7)	229±32 (7)	16.3±5.5 (7)	0.8±0.4 (7)	0.19±0.05 (7)	0.34±0.14 (7)
Side	*M. mirabilis*	5	0.26±0.02 (11)	257±68 (11)	19.1±8.4 (11)	1.3±0.5 (11)	0.21±0.06 (11)	0.52±0.14 (11)
		10	0.26±0.02 (11)	219±44 (11)	14.5±3.5 (11)	0.9±0.2 (11)	0.19±0.05 (11)	0.45±0.14 (11)
		25	0.27±0.02 (8)	178±24 (8)	14.7±5.5 (8)	0.8±0.3 (8)	0.22±0.06 (8)	0.44±0.11 (8)
	M. pharensis	5	0.27±0.02 (9)	262±64 (9)	8.3±4.6 (9)	0.5±0.3 (9)	0.09±0.04 (9)	0.20±0.09 (9)
		10	0.27±0.02 (10)	214±35 (10)	8.9±3.6 (8)	0.4±0.2 (8)	0.12±0.05 (8)	0.18±0.05 (8)
		25	0.26±0.03 (7)	171±47 (7)	9.0±3.4 (7)	0.3±0.1 (7)	0.14±0.03 (7)	0.18±0.04 (7)
	M. senaria	5	0.25±0.01 (8)	229±36 (8)	6.6±1.9 (8)	0.4±0.2 (8)	0.08±0.03 (8)	0.17±0.09 (8)
		10	0.27±0.02 (9)	179±39 (9)	5.7±2.3 (9)	0.3±0.1 (9)	0.09±0.05 (9)	0.18±0.06 (9)
		25	0.25±0.02 (8)	159±37 (8)	5.7±1.9 (8)	0.2±0.1 (8)	0.10±0.03 (8)	0.15±0.03 (8)

0.001; Figure 3.4p), suggesting that, for instance, polyp density and β,β-carotene Chl a^{-1} reach the highest values in *M. formosa* and in colonies harbouring symbiont type B15. Symbiont type B13 never differed from type B7 (Figure 3.4d, h, l and p).

If the PCA and SCoTLASS are run without previous outlier removal (n = 179), very similar SCs result that further confirm the previously described univariate significances (except for the minor SC4). In addition, to include symbiont cell-size data and Chl *a* cellvol^{-1} in the analyses, a new PCA was run for a sample set (71 colonies) that only included data from α = 0° colony top positions. The results were similar to the earlier analyses. After SCoTLASS (t = 2.648), each SC represents the same variables, except that some parameters loading in SC1 and SC3 have swapped positions, for instance, dinoxanthin Chl a^{-1} and xanthophylls Chl a^{-1} load on SC1. The two new variables, cell size and Chl *a* cellvol^{-1}, strongly load on SC4 (positively correlated with, e.g., β,β-carotene Chl a^{-1}) and SC3 (positively correlated with, e.g., peridinin Chl a^{-1}), respectively. The statistical significance of the explanatory variables (now excluding colony surface position) is similar to the full model significance, but SC1 and SC2 also relate to depth besides host species, and SC3 relates only to depth.

Overall, the results of the full model show that SC3 is the most sensitive component (responds to all explanatory variables). SC1 is exclusively environment related, while SC2 and SC4 are typically host- and/or symbiont-dependent components. Host species arises as the most important explanatory factor; it is highly statistically significant to three of the four SCs considered (exception is SC1). Colony surface position and depth follow in the scale of decreasing significance. Finally, symbiont genetic type is the factor that explains the

least variance as it only relates statistically to the last two (minor) components. Table 3.3 summarizes the analyses, showing the four SCs, the main mechanisms they represent, and the respective statistical outcomes.

Discussion

The combination PCA-SCoTLASS was successful in enhancing interpretability, and the identical results obtained from different approaches confirm the robustness of the data. Each SC represents a distinct set of variables, supposedly indicating different underlying photobiological mechanisms ranging from more environmentally controlled to more genetically constrained.

Light environment: Depth and colony surface position

Within-colony landscape, here represented as either $\alpha = 0°$ or $\alpha = 90°$ colony surface, appears to account for the same kind of effect as depth. This interpretation is supported by the link in statistical significance between depth and surface position. In addition, a PCA including only data originating from $\alpha = 0°$ colony surface yielded similar results to the full model. This suggests that depth and surface position basically represent the same environmental parameter: light. The analysis strongly highlights the dependence of photochemical, photosynthetic efficiencies, and derived parameters on light (SC1). The increase in light-use efficiencies when moving to deeper (or darker) habitats has been documented in several studies with corals (Gorbunov *et al.* 2001; Warner *et al.* 2006) and reflects photoacclimation. This is confirmed by the adjustment of the optimal irradiance for photosynthesis (E_k). This general trend toward darker environments is also supported by other mechanisms (SC3), such as the increase in Chl *a* cell^{-1} or peridinin Chl *a*$^{-1}$, and the decrease in *ETRmax*, indicating a higher light-harvesting

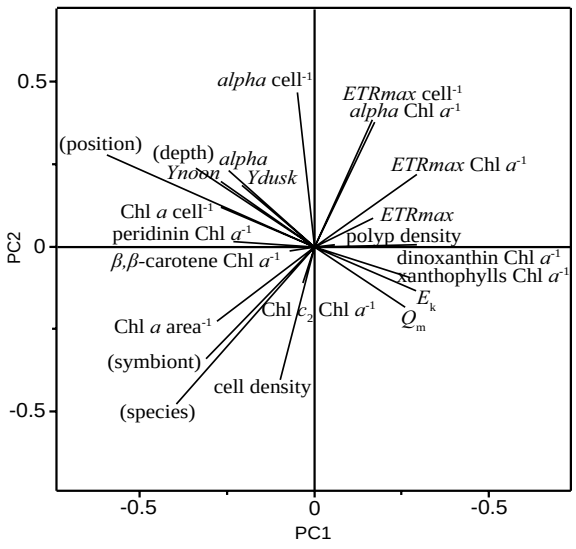

Figure 3.2 *Madracis* spp. photobiological data PCA correlation biplot for first two components (PC1 and PC2). For abbreviations, *see* Table 3.1. Explanatory variables - host species, depth, colony surface position and symbiont genetic type (in brackets) - are superimposed using cross-correlations.

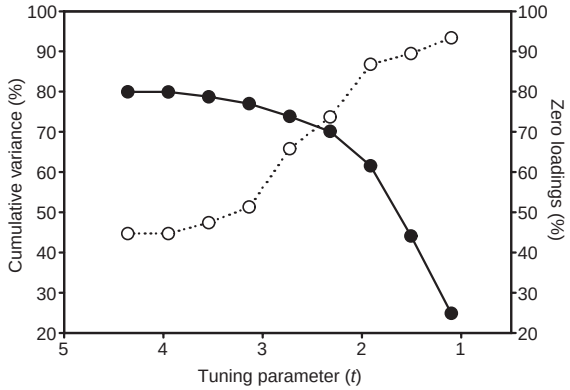

Figure 3.3 SCoTLASS analysis. Cumulative variance explained by the first four PCs (solid line) and the percentage of zero loadings in those components (dotted line) as the tuning parameter decreases (t = 4.359 corresponds to PCA).

capacity under conditions of light limitation and higher photosynthetic production in the presence of light. The increase in peridinin Chl a^{-1} suggests a broader absorption spectrum of the phototrophic component into the greenish region in order to maximize photosynthesis. Q_m, the maximum excitation pressure over PSII, has been used as a proxy of algal physiological state and is known to be covariant with NPQ (Iglesias-Prieto *et al.* 2004). This phenomenon is reported to cause the relative suppression of photosynthesis, reaching its highest level around solar noon (Hoegh-Guldberg and Jones 1999). If the excess of absorbed energy is too high, it may overwhelm such protective mechanisms, and PSII photodamage, or photoinhibition, can occur (Gorbunov *et al.* 2001). High Q_m levels, such as the ones we measured in shallow water, also reflect increasing potential for photoinhibition and, ultimately, bleaching (Warner *et al.* 2006). SC3 also represents the pigments involved in the xanthophyll cycle, which constitutes one of several protective mechanisms associated with NPQ (Muller *et al.* 2001). The decrease of xanthophyll-cycle pool with depth and from $\alpha = 0°$ to $\alpha = 90°$ over colony surface has long been known to be related to decreasing irradiance (Titlyanov 1981; Brown *et al.* 1999). Dinoxanthin shows the same trend, confirming the photoprotective function of this carotenoid. NPQ and photoinhibition are two hypothetical explanations for the dramatic drop of *ETRmax* that we measured at 5-m depth for $\alpha = 0°$ surface of all species (Table 3.1). Cell density (SC2) is not strongly environmentally controlled, confirming other studies that have reported that algal densities do not show changes over light gradients (Falkowski and Dubinsky 1981; Jones and Yellowlees 1997). Still, there is variation related to depth and surface position (*see* also Table 3.1). For example, the slight tendency of decrease we measured for symbiont densities with increasing depth could be linked to a general decrease of host-tissue biomass toward the deeper reef (McCloskey and Muscatine 1984; Fitt *et al.* 2000). Overall, this study highlights the importance of depth- and surface position-related light habitats in the photobiology of corals and their symbionts.

Host species and symbionts

Results also point to an important role of species-specific traits in controlling the photobiological response of the association. Here, the key adaptive factor that explains most variation appears

Table 3.2 Loadings (and percentage of cumulative variance) for the first four PCs obtained by PCA and for the respective SCs obtained by SCoTLASS (with $t = 2.322$). Each entry corresponds to one of the original 19 variables. For abbreviations, *see* Table 3.1. Values in bold represent strong correlations (loading > 0.2) between original variables and new components.

Variables	PC1	PC2	PC3	PC4	SC1	SC2	SC3	SC4
Cell density	-0.10	**-0.41**	**-0.20**	**0.29**	0.00	**-0.37**	0.02	-0.10
Chl *a* area^{-1}	**-0.30**	**-0.23**	0.07	0.18	0.00	**-0.46**	0.00	0.07
Chl *a* cell^{-1}	**-0.29**	0.12	**0.30**	-0.06	0.02	0.00	**-0.54**	0.12
Chl c_2 Chl a^{-1}	-0.03	-0.11	**-0.45**	-0.17	0.00	0.00	0.00	**-0.61**
Peridinin Chl a^{-1}	**-0.25**	0.02	0.02	**-0.36**	0.00	0.00	**-0.51**	-0.15
β,*β*-carotene Chl a^{-1}	-0.07	-0.01	**0.58**	0.14	0.00	0.00	0.00	**0.66**
Dinoxanthin Chl a^{-1}	**0.31**	0.01	-0.15	0.09	-0.03	0.00	**0.55**	0.00
Xanthophyll-pool Chl a^{-1}	**0.29**	-0.09	-0.08	0.03	-0.12	0.00	**0.31**	0.00
Polyp density	0.06	0.01	**0.28**	**0.45**	0.00	0.00	0.00	**0.35**
Ydusk	**-0.22**	0.19	-0.14	**0.29**	**0.24**	0.00	0.00	0.00
Ynoon	**-0.29**	**0.20**	**-0.22**	0.19	**0.55**	0.00	0.11	0.00
Q_m	**0.28**	-0.18	**0.23**	-0.13	**-0.50**	0.00	0.00	0.01
ETRmax	0.18	0.09	-0.08	**0.52**	0.00	0.00	**0.20**	0.00
alpha	**-0.26**	**0.23**	-0.17	**0.25**	**0.48**	0.00	0.00	0.00
E_k	**0.31**	-0.13	0.06	0.11	**-0.39**	0.00	0.00	0.00
ETRmax cell^{-1}	0.18	**0.39**	0.13	0.00	0.00	**0.46**	0.00	0.04
ETRmax Chl a^{-1}	**0.31**	**0.22**	-0.08	0.04	0.00	**0.44**	0.03	-0.05
alpha cell^{-1}	-0.05	**0.47**	0.09	-0.10	0.00	0.10	-0.06	0.15
alpha Chl a^{-1}	0.18	**0.38**	-0.16	-0.05	0.00	**0.49**	0.00	-0.03
Cumulative variance (%)	40.5	62.8	72.6	79.9	22.8	45.3	61.1	70.1

to be symbiont cell density, or better, the genetic factors controlling it. Symbiont density is thought to be regulated by limitation in space (Drew 1972). Any other factors controlling symbiont cell size can also indirectly determine algal densities (Jones and Yellowlees 1997). Cell size is reported to be symbiont-specific (LaJeunesse *et al.* 2005), and our data show that this could also be the case for *Symbiodinium* types B7, B13 and (the larger cell-sized) B15. Thus, based on the *Madracis* model, we propose that coral tissue space availability (thickness) and symbiont cell size are relatively genetically constrained and that both parameters ultimately regulate cell density. For instance, in *M. pharensis*, the two-fold depth decrease in cell numbers (*see* Table 3.1) is caused by the depth-based symbiont replacement of type B7 by the larger type B15 (Frade *et al.* 2008c). In addition to cell-size differences, symbiont types also relate to pigment parameters such as Chl *a* cell^{-1}, peridinin Chl a^{-1}, dinoxanthin Chl a^{-1}, and xanthophylls Chl a^{-1} (SC3) or *β*,*β*-carotene Chl a^{-1} and Chl c_2 Chl a^{-1} (SC4). This is an *in situ* indication suggesting that symbiont ITS2 types correlate with functional properties and may represent distinct species. The presence of *Symbiodinium* type B15 at greater depths relates to phenotypic differences and may have an adaptive role, eventually allowing for a deeper lower limit of distribution in *M. pharensis* and *M. formosa* (Vermeij and Bak 2003). Types B7 and B13, on the other hand, are typical for shallower environments and exhibit a high photoprotective component. Such symbiont-specific differences in thermal-dissipation mechanisms have been suggested elsewhere (Iglesias-Prieto and Trench 1997b; Robison and Warner 2006). The absence of physiological differences between types B7 and B13, in addition to their close genetic relatedness (Frade *et al.* 2008c), suggests that they do not represent ecologically distinct forms or species.

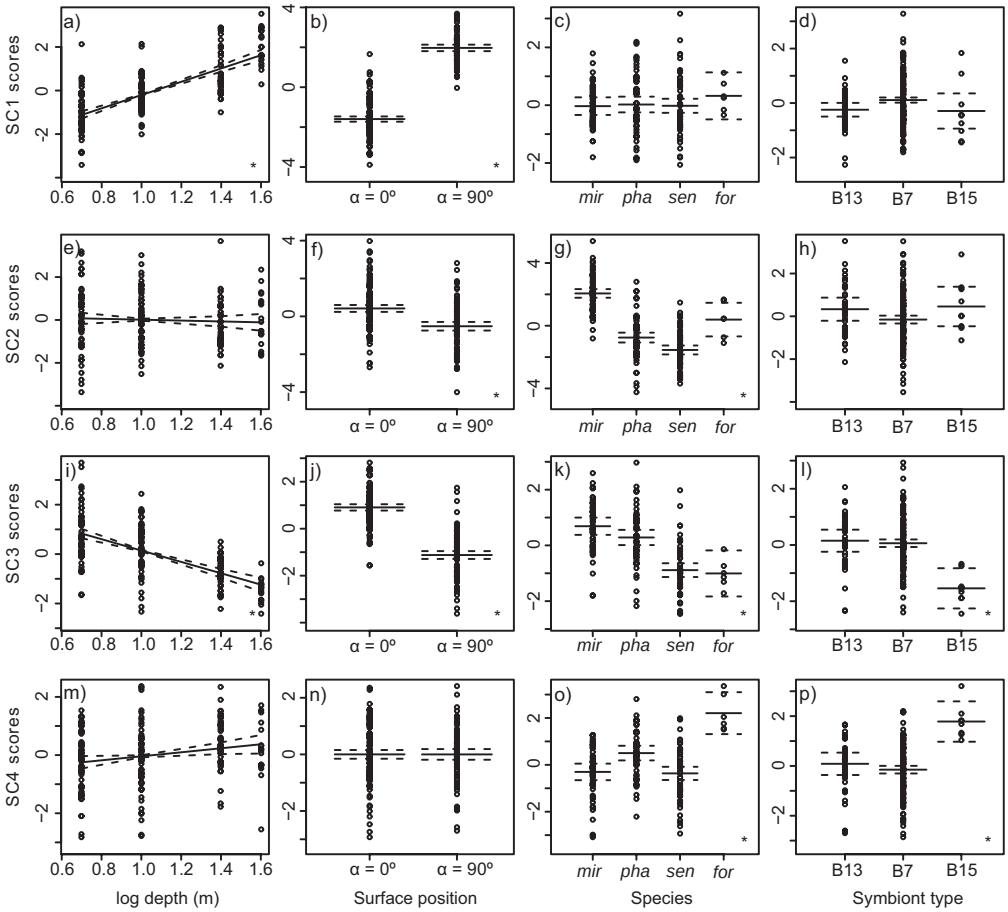

Figure 3.4 SC score variation among (**a**, **e**, **i**, **m**) depth, (**b**, **f**, **j**, **n**) colony surface position, (**c**, **g**, **k**, **o**) host species (*mir* = *M. mirabilis*, *pha* = *M. pharensis*, *sen* = *M. senaria*, and *for* = *M. formosa*), and (**d**, **h**, **l**, **p**) symbiont type. Depth was log-transformed. Lines represent (solid) mean and (dotted) 95% confidence intervals. Statistically significant linear regressions are marked with * (right bottom corner). Note that part of the original variables correlate negatively with the SCs (*see* Table 3.2).

Besides differing in symbiont cell density, *Madracis* host species also relate to the aforementioned photosynthetic parameters (represented by SC3 and SC4). The origin of such differences in photosynthetic rate or accessory harvesting and photoprotective pigment contents could lie in an acclimation response to the amount of light absorbed by the algal symbionts they harbour (or the photosynthetic units themselves) and/or be due to inadequate nutrient supply to the symbiont. Alternative mechanisms controlling the availability of light at the symbiont cellular level could include specific differences in skeletal multiple scattering (Enriquez *et al.* 2005), host pigment composition (Schlichter *et al.* 1994; Salih *et al.* 2000), or photosynthetic pigment self-shading (Dubinsky *et al.* 1984). This last alternative mechanism for controlling light, variation in photosynthetic pigment self-shading, is supported by our findings, which show host-specific differences in terms of symbiont cell density. In fact, host-species differences in SC2 and SC3 follow opposite trends: *M. mirabilis* resulted in the lowest symbiont densities and the highest *ETRmax*, highest activity of photoprotective xanthophylls, and the lowest Chl *a* cell^{-1}, while *M. senaria* showed the opposite and *M. pharensis* was

Table 3.3 Main photobiological mechanisms involved in each of the four SCs and statistical significance of depth, colony surface position, host species, and symbiont type.

Component	Main mechanism	Depth	Position	Species	Symbiont
SC1	Photoacclimation: light use efficiency	Increasing with increasing depth	Increasing from top to side	No significant effect	No significant effect
SC2	Symbiont cell densities and pigment self-shading	No significant effect	Increasing from top to side	Highest in *M. senaria* and *M. pharensis*	No significant effect
SC3	Photoprotective pathways (and sensitive accessory pigments)	Decreasing with depth	Decreasing from top to side	Highest in *M. mirabilis* and *M. pharensis*	Higher in types B7 and B13 than in B15
SC4	Polyp density and genetically fixed accessory pigments (*β,β*-carotene)	No significant effect	No significant effect	Highest in *M. formosa* and *M. pharensis*	Higher in type B15 than in B7 and B13

intermediate.

Specific differences in cell density may also be coupled to nutrient supply (Dubinsky *et al.* 1990). Nitrogen limitation, for instance, is know to interfere with the efficiency of transfer of absorbed light energy to the PSII reaction centres due to the loss of reducing power sinks, thereby inducing the requirement for increased energy dissipation (Verhoeven *et al.* 1997). In this respect, species differences in photoprotective pigment contents, an indication of specific needs for heat dissipation, contrast with stable NPQ throughout the genus (estimated by Q_m). This diverges from other *in situ* studies in which Q_m differences among host species varied from large (Iglesias-Prieto *et al.* 2004) to small (Warner *et al.* 2006). The disengagement between NPQ and xanthophyll pool highlights the idea that photoprotection is also dependent on other important mechanisms, such as the activity of antioxidant enzymes (Levy *et al.* 2006b) or the ability to repair PSII (Warner *et al.* 1999). Finally, polyp density typically constitutes a host-specific characteristic. This could potentially relate to skeleton-mediated modulation of light available to the endosymbionts within the tissue (Enriquez *et al.* 2005).

Holobiont strategies

Linkages between the photobiological response of hosts and symbionts and their distribution and dominance over the reef slope suggest distinct holobiont strategies. Vermeij and Bak (2002) described the distribution of the *Madracis* genus relative to light regimes, irrespective of depth, and found that the branching species, including *M. mirabilis* and *M. formosa*, have a preference for maximum light capture, while more massive morphologies, such as *M. pharensis* and *M. senaria*, preferably occupy shaded positions. Other studies suggest that branching species have faster growth rates than massive morphologies (Gates and Edmunds 1999). The lower symbiont biomass in the branching *M. mirabilis* and *M. formosa* may be related to limited host-tissue space availability. Hypothetically, this could force these species to occupy well-lit habitats to maximize photosynthesis and eventually achieve the production necessary for its growth and maintenance. Massive species, containing a larger phototrophic biomass, on the other hand, may achieve their photosynthetic budget while avoiding extreme light exposition. Increased skeletal complexity in branching species may also contribute to the intensification of the local irradiance and therefore to an increase of the absorption efficiency

by the algal endosymbionts (Enriquez *et al.* 2005). Although good absorption estimates are not available, our results suggest that *M. mirabilis* has very high photosynthetic production (as estimated by relative *ETR*), as opposed to *M. senaria*. Skeletal isotopic composition data show that *M. mirabilis* has the strongest metabolic ^{13}C enrichments caused by photosynthesis within the genus (Maier *et al.* 2003). Such high photosynthetic production could be related to observed host behavioural differences such as diurnal polyp extension (P.R. Frade, pers. obs.; Veron 2000), which contributes to a higher carbon availability (Levy *et al.* 2006a). Furthermore, Vermeij *et al.* (2002) detected host green fluorescence in most *Madracis* species but not in *M. mirabilis*, and although the exact function of host pigments such as green fluorescent proteins is still uncertain (Wiedenmann *et al.* 2004), the *Madracis* species depth distribution argues for the possibility that these pigments have a photoenhancing function (Schlichter *et al.* 1994), rather than a protective one (Salih *et al.* 2000). Although the reasons for the upper limit of the depth distribution of *M. formosa* (the other branching species, occurring below 30 m) are uncertain, these could include slow metabolism and lower competitiveness, which would only allow for the colonization of relatively open ecological niches.

In summary, we find opposing holobiont strategies in the *Madracis* genus, where the two extremes are represented by *M. senaria* and *M. mirabilis*. Symbiont diversity, *per se*, cannot explain such strategies. On one side, there is *M. senaria*, which harbours high densities of symbionts that are self-shading, creating a low-light intratissue environment and a reduced need for photoprotective pathway activation. These symbiotic associations have physiological properties favouring the enhancement of light harvesting and can be expected to successfully colonize deep or shaded habitats. In very shallow water, they are probably limited by oxidative stress resulting from extreme light excitation (note the highest Q_m was measured for *M. senaria* at 5 m; *see* Table 3.1), a phenomenon supposed to influence the upper limit of distribution of scleractinians (Hoogenboom *et al.* 2006). In our sampling approach, purposely limited to exposed colonies to fully capture the depth-light effect, the *M. senaria* samples collected at 5-m depth are part of the rare conspecific colonies at that depth that occupy noncryptic habitats. On the other side, there is *M. mirabilis*, which represents associations harbouring relatively low symbiont and pigment densities, hypothetically depending on chronic photoprotective mechanisms. These species are probably high-light adapted, and their distribution is limited by low light levels. *Madracis pharensis*, a dominant depth-generalist, has intermediate characteristics. This species appears to be broadly light-adapted, a phenomenon possibly related to the change in symbiont type with depth (Frade *et al.* 2008c).

Final considerations

This study constitutes one of the most extensive holistic approaches to the study of photophysiology of coral-algal symbioses. The multivariate statistical analysis highlights the central role of irradiance in the biology of corals and their symbionts. It reveals general photobiological components underlying distinct sets of variables, some of which (photochemical or photosynthetic efficiencies and linked parameters such as Q_m, *alpha* or E_k) are more sensitive to environmental changes, while others (such as symbiont cell size or polyp density) are more genetically constrained. Such distinction between acclimatisation and adaptation mechanisms has important consequences for predicting coral resilience in a rapidly changing environment (Hoegh-Guldberg *et al.* 2007). The broad plasticity demonstrated for several parameters (such as for photochemical efficiencies) ultimately reflects high adaptation

to the reef environment and its light gradients. The results emphasize the trade-offs among different holobiont strategies, which appear to differ in the physiological optimization of light-harvesting and protective mechanisms. The distinct host specificity and depth distributions previously reported in symbiont ITS2 types in the *Madracis* genus (Frade *et al.* 2008c) are now shown to relate to distinct *in situ* physiological activity. This highlights symbiont niche diversification and the role of symbiont functional diversity in the adaptation of reef-building corals.

Our study underscores that corals are complex organisms and that both symbiotic partners contribute to the physiological response of the whole association. However, symbiont functional diversity, *per se*, does not appear to regulate coral distribution in the *Madracis* genus, emphasizing the importance of species-specific morphological and physiological properties of the coral host in vertical distribution patterns.

Acknowledgements

We are grateful to Francisca Vermeulen for helping with sample collection and coral surface area determination, Eilke Berghuis for HPLC support, Marcel Veldhuis for flow cytometer support, Berber van Beek for cell-size measurements, Gerard Nieuwland for logistic support, and Jeandra de Palm and Osric Wanga from the Analytisch Diagnostisch Centrum (ADC) in Curaçao for the use of freeze-drier and freezers. This research was funded by the Portuguese Science and Technology Foundation (FCT, Portugal), through a PhD grant (SFRH/BD/13382/2003) to P.R.F. L.T. was financially supported by the Earth and Life Sciences Foundation (ALW), which is subsidised by the Netherlands Organization for Scientific Research (NWO).